Pergamon

Int. J. Multiphase Flow Vol. 24, No. 4, pp. 617–634, 1998

Printed in Great Britain
PII: S0301-9322(97)00060-8
0301-9322/98 $19.00 + 0.00

TOMOGRAPHIC IMAGING OF THE PHASE DISTRIBUTION IN TWO-PHASE SLUG FLOW

N. REINECKE, G. PETRITSCH, M. BODDEM and D. MEWES†
[1]Institute for Process Engineering, University of Hannover, Hannover, Germany

(Received 31 December 1996; in revised form 30 July 1997)

Abstract—A new tomographic measurement technique for the spatial imaging of the phase distribution in horizontal slug flow is presented. The features of the new technique are a high spatial and temporal resolution. The measurement principle is based on the measurement of the conductivity between parallel wires. It is a function of the liquid hold-up between the wires. Using three different measurement directions, projections with linearly independent integral measurements of the phase distribution are obtained. These are processed using an iterative series expansion method based on the algebraic reconstruction technique (ART). The quality of the reconstruction is increased using a priori knowledge of the flow regime. The maximum temporal resolution is 5 ms and the spatial resolution is smaller than 1% of the cross-sectional area of the pipe. © 1998 Published by Elsevier Science Ltd. All rights reserved

Key Words: tomography, two-phase flow, slug flow, phase distribution

1. INTRODUCTION

Multiphase flows of gas, vapor and liquid are encountered in a variety of different chemical reactors, power plants and transportation pipelines. The integral fluid dynamic properties in these systems, i.e. superficial velocities, pressure drop and residence time distribution, are largely influenced by the phase distribution inside the pipeline. The phase distribution itself is a function of the geometric boundary conditions of the flow field, the volumetric flowrates and physical properties of the phases (Nädler and Mewes 1995a,b; Gregory and Scott 1969; Herm-Stapelberg and Mewes 1994).

In horizontal pipelines, one of the most predominant flow regimes is the slug flow. Besides integral parameters like superficial velocities and physical properties of the phases as well as pipeline diameter, the pressure drop encountered in horizontal slug flow is strongly influenced by the volumetric liquid hold-up and the distribution of the liquid phase inside every individual cross-sectional area. Up to date, either only integral measurements of the liquid hold-up or local measurements conducted with intrusive probes have been used (Jones and Delhaye 1976; Delhaye 1978). Using local probes, a measurement of the liquid hold-up at several positions at the same time is impossible. For this measurement task tomographic techniques have to be used.

2. SLUG FLOW IN HORIZONTAL PIPELINES

In cocurrent horizontal two-phase flow in general four major flow regimes are distinguished. These are the stratified flow, the plug flow, the slug flow and the annular flow. These and additional flow regimes as well as the flow regime boundaries, pressure drop and general phase distributions have been studied by several authors (Hewitt 1991).

The most predominant flow regime encountered in technical applications, as for example the exploration of submarine resources, is slug flow. In figure 1(a) the phase distribution of the gas and the liquid phase encountered in slug flow is depicted schematically. The slug unit consists of the slug zone and the trailing film zone. Within the slug zone the front is often referred to as the mixing zone.

†To whom correspondence should be addressed.

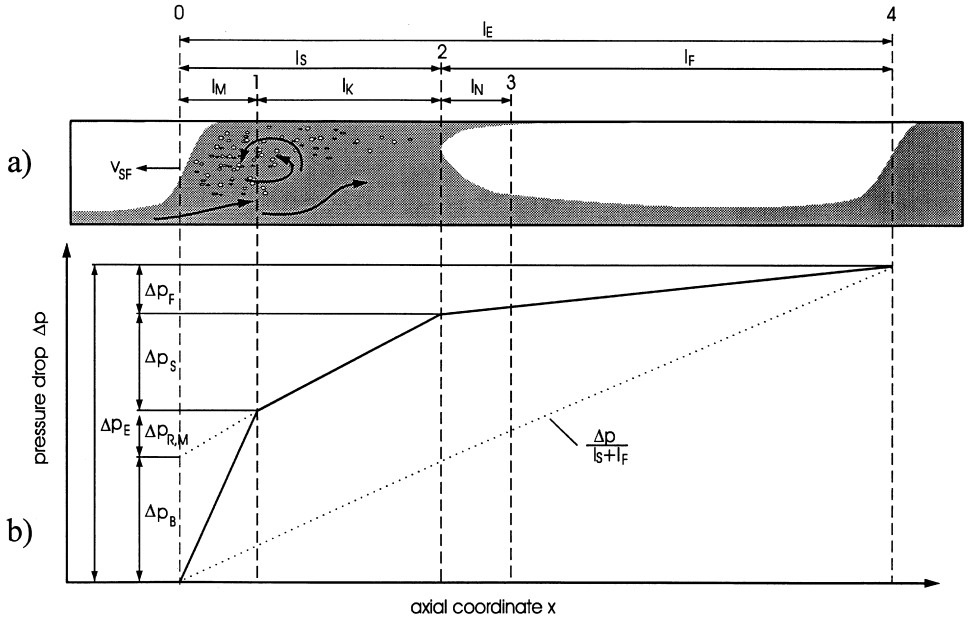

Figure 1. Schematic representation of a slug unit (a) and the pressure drop along a slug unit (b).

The pressure drop along the slug plotted in figure 1(a), which in turn is schematically plotted in figure 1(b) has been calculated, for example by Gregory and Scott (1969). In order to do the calculation, the following properties have to be known:

- the length of the slug unit including the distinction between slug and film zone as well as the distinction within the slug zone between mixing and core zone;
- the void fraction in the slug and the film zone;
- the average slug velocity as well as the slug front velocity and the average film velocity;
- the slug frequency.

Azzopardi *et al.* (1985) conduct a thorough comparison between existing pressure drop correlations and measured data. They show that the knowledge of the void fraction of the flow has a large influence on the accuracy of the model as also stated by Begs and Brill (1973). The pressure drop equation given by Dukler and Hubbard (1975) is based on the fact that the pressure drop of the film zone between two slug zones can be neglected compared to the pressure drop of the slug zone. In figure 1(b) the pressure drop of the slug unit is plotted schematically. The pressure drop generated in the mixing zone contributes to about 50% of the total pressure drop of the slug unit. In figure 2 the measured pressure drop of single individual slugs is plotted as a function of the slug velocity. The measurements have been conducted with the experimental set-up described in Section 4. In the transition region between the plug and the slug flow the pressure drop of the slug unit decreases with increasing slug front velocity. Such a pressure drop characteristic has also been reported by Ozawa *et al.* (1989) for the two-phase flow in a capillary. There, the region with the negative dependence of the pressure drop on the flow velocity is explained by the transition from bubbly flow to slug flow. We assume, that for horizontal two-phase flow the negative dependence of the pressure drop on the flow velocity is due to the entrainment of gas into the slug unit, which has to be proved by further investigations.

Experimental investigations on the dispersion of gas into the front of the slug are conducted by a number of authors. Nydal and Andreussi (1991) are measuring the void fraction of single slugs using flush mounted ring-electrodes. The experimental set-up consists of a pipe with 50 mm diameter and 17 m length. The inclination is 3° against the horizontal. The dispersion of the gas into liquid is only observed when the velocity of the slug reaches a critical value and sufficient liquid in form of the film is present. Jepson and Taylor (1993) are conducting their experiments on the void fraction in the slug in a pipe with 300 mm inner diameter.

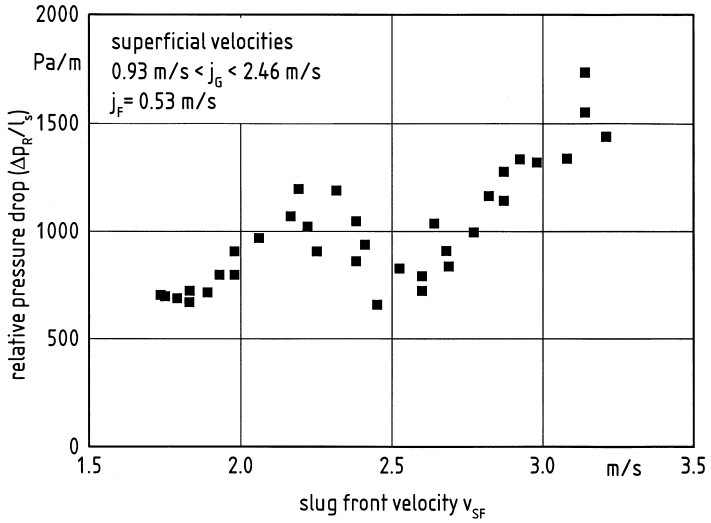

Figure 2. Pressure drop of individual slugs as a function of the slug front velocity.

The equations developed for the calculation of the void fraction inside the mixing and core zone can be grouped into three different approaches. The first group consists of empirical equations without discrimination of the flow regime. An overview of these correlations is given by Spedding *et al.* (1988). From his experimental investigations he concludes that the accuracy of the equations depending on flow regime and flow system is satisfactory.

A second group of equations consist of simple physical models corrected using experimental results. Frequently employed equations include the one from Gregory *et al.* (1978). This equation is based on experimental investigations using an oil-air-system in pipes with 25.8 and 51.2 mm diameter.

In contrast to the models from the first two groups, the equations of the third group are based on physical models of the entrainment of the gas and the dispersion and distribution of the gas within the liquid. The model developed by Barnea and Brauner (1985) is based on the assumption that the dispersed gas phase behaves like bubbles. The void fraction in the liquid slug then corresponds to the void fraction of a bubbly flow with the same mixture velocity at the transition to slug flow. Experimental investigations are conducted by Andreussi and Bendiksen (1989). They vary the physical properties of the phases and the pipe diameter. The results are compared with a semi-empirical relationship. The physical basis of the correlation is the assumption that the amount of gas entrained at the front of the slug is equal to the amount deentrained at the back. The volumetric void fraction in the slug is calculated by the volumetric gas flow deentrained from the roll wave of the mixing zone into the leading bubble. The parameters of the model are fitted to the experimental data. The agreement between model and experiment is good. According to Andreussi and Bendiksen (1989), there is a large influence of the surface tension and the gas density on the void fraction within the slug.

From the referred papers it is evident, that the intensity of the mixing and thus the phase distribution as well as the gas entrainment and integral void fraction in the individual slugs are dependent on a number of factors. There are the liquid velocity in the film zone and in the slug zone, the velocity of the gas phase in the film zone, the physical properties of the phases, the diameter of the pipe and the inclination.

Even though a lot of work has been done on this subject, a prediction of the critical slug velocity for the onset of gas entrainment is not possible. In all the experimental investigations, the void fraction within the slug has only been measured using integral measurement techniques. Therefore, no information on the local phase distribution is possible. It is also not possible to link the void fraction and its distribution to the pressure drop for a single slug or the complete slug flow. Therefore, in the present investigation a new tomographic measurement technique for the measurement of the void fraction distribution is used.

3. TOMOGRAPHIC MEASUREMENT TECHNIQUE

The measurement of multi-dimensional physical properties using tomographic measurement techniques requires the performance of two steps. First, a number of linearly independent integrals or projections of the unknown property distribution are generated. In a second step, the local distribution of the property, which is contained in the integral projection, is calculated using mathematical reconstruction algorithms. For the measurement of the integral projections a number of physical measurement principles can be used. These are for example X- or γ-ray techniques (Ikeda *et al.* 1983), microwaves (Adams and Anderson 1982), ultrasound, coherent and white light (Mewes and Fellhölter 1993; Ostendorf and Mewes 1988; Mewes *et al.* 1989), nuclear magnetic resonance (NMR) (Gladden 1994) and positron emission (PET) (Simons *et al.* 1993). Due to the necessary high frequencies (100 Hz and more), the restricted optical transparency and the phase boundaries present in the measurement volume these techniques are not applicable for the tomographic imaging of the phase distribution in slug flow. For this measurement task, electrical techniques like capacitance and conductance tomography have to be used.

In capacitance tomography the measurement principle is based on the dependence of the externally measurable capacitance between electrodes mounted peripherally around the measurement volume on the value and the distribution of permittivities inside the measurement volume. In two-phase flow, the values are those of the gas and the liquid phase and the distribution is those of the phases. Using a number of electrodes mounted peripherally around the measurement volume, different combinations and thus linearly independent measurements are made (Xie *et al.* 1995; Reinecke and Mewes 1994). For the measurement of the capacitance, an axial extension of the electrodes is required, generating a measurement volume rather than a plane. With extended phase boundaries inside the measurement volume, the electrical field properties become discontinuous and the reconstruction of the phase distribution erroneous.

For conductive tomography techniques currently used, the electrodes are also mounted peripherally around the measurement volume. They are mounted flush with the wall and in direct electrical contact with the flowing fluid phases (Wang *et al.* 1994; Abdullah 1993). Depending on the technique, either a constant current is induced and the resulting potential at the other electrodes is measured or a constant potential is applied to two electrodes and the resulting current measured. Therefore, the electrical properties measured are non-linearly dependent on the phase-distribution. In addition, this technique requires the full contact of the electrodes with the conducting phase. This requirement cannot be fulfilled for the horizontal slug flow in the region of the film zone. Therefore, for the present investigation, a new arrangement of the electrodes is generated.

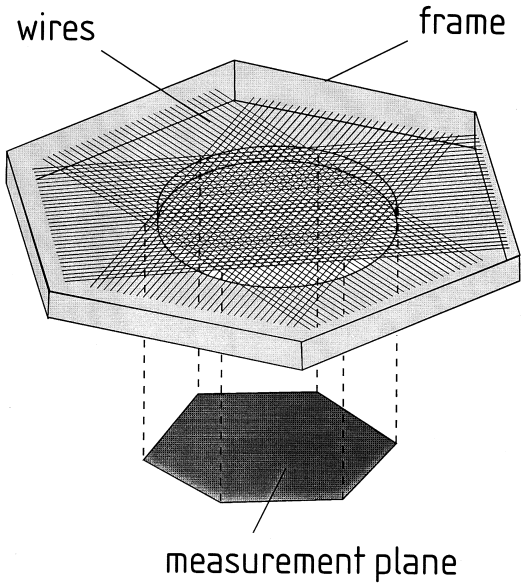

Figure 3. Schematic representation of the new sensor.

3.1. *New measurement technique*

In figure 3 the new sensor for the conductive tomography is depicted schematically. In three close parallel planes sets of parallel wires are strung across the cross-sectional area of the pipe. The planes are set $h = 3$ mm apart. In every plane a total of 29 wires with a diameter of 100 μm are arranged. With a distance between parallel wires of $a = 2$ mm a total free cross-sectional area through the sensor of $\varphi > 95\%$ is achieved. Due to the extremely small diameter of the wires the flow is not disturbed and the additional pressure drop negligible. The measurement principle is based on the conductance between two parallel wires. This is a function of the electrical properties and the distributions of the phases. In figure 4 this relationship is given schematically. According to the given phase distribution, liquid bridges the gap between the wires in several positions. The size on the number of the liquid bridges is dependent on the phase distribution. The arrangement can be simplified by an arrangement of ohmic resistors in parallel. Neglecting the conductivity of the gaseous phase, the measurable conductance G_M becomes

$$G_M = \sum_{i=1}^{n} \frac{1}{R_i}. \quad [1]$$

In [1] R_i is the resistance of a discrete liquid bridge between the wires. This resistance of a bridge with dimension l_i is given by

$$R_i = \frac{1}{G_{max}} \frac{l}{l_i} \quad [2]$$

with l as the total length of the pair of wires and G_{max} the conductance between the wires when completely wetted by the liquid. Therefore, the measurable conductance becomes

$$G_M = G_{max} \sum_{i=1}^{n} \frac{l_i}{l}. \quad [3]$$

Rearrangement of (3) leads to

$$G^* = \frac{G_M}{G_{max}} = \frac{\sum_{i=1}^{n} l_i}{l}. \quad [4]$$

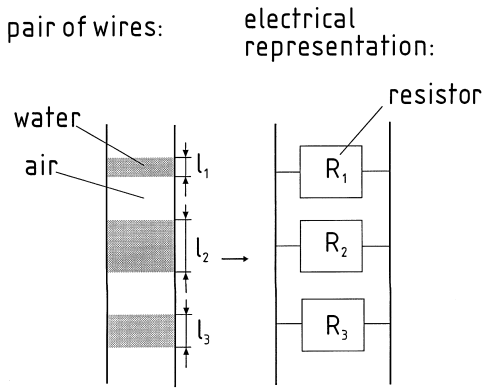

Figure 4. Schematic representation of the relationship between the phase distribution and the measurable conductance between two parallel wires.

The ratio of the wetted length to the total length of the wire equals to the liquid hold-up, thus

$$G^* = 1. \qquad [5]$$

The relative conductance G^* is equal to the integral measurement value Φ_M given in [1]. By measuring the conductance between the parallel wires a total of 28 linearly independent measurements of the distribution of the liquid hold-up is obtained. Using the three parallel planes of wires a total number of three projections is available.

In order to avoid the influence of the conducting wires on the measurement of the integral conductance the planes of parallel wires are arranged with an axial offset. In figure 5 the relative conductance of two fully wetted wires is plotted as a function of the relative distance of the planes. For a relative distance of 1.4 the influence of the conducting wires of one plane on the measurement of the integral conductance in another plane is smaller than 2%.

The measurement of the conductance between the two parallel wires is obtained using a commercial impedance meter. The measurement is done using an AC-bridge with a carrier frequency of 1 MHz and a voltage amplitude of 0.2 V ($\pm$0.1 V). Using a phase-sensitive demodulation of the resulting signal, an independent measurement of the real components of the impedance is possible. Since a voltage is actively driven onto the wires, a parallel measurement of several pairs is impossible due to the electromagnetic field interference. Therefore all pairs of wires have to be sampled sequentially. This sequential sampling is achieved with a newly developed multiplexing circuit which is driven by the digital output from a PC. The complete measurement chain of the technique is given in figure 6.

3.2. *Reconstruction*

The ultimate goal of the reconstruction is the inversion of [1] for all projections, yielding the desired phase distribution within the measurement plane. Due to the limited number of projections a direct inversion or a convolution and backprojection (Rowland 1979) is not possible. The reconstruction is further complicated due to the severe underdetermination of the set of equations since there are usually a greater number of points to be reconstructed than number of measurement values.

For the reconstruction of an unknown phase distribution $\varepsilon(x, y)$, an iterative reconstruction procedure based on a series expansion method is used. The algorithm is schematically plotted in

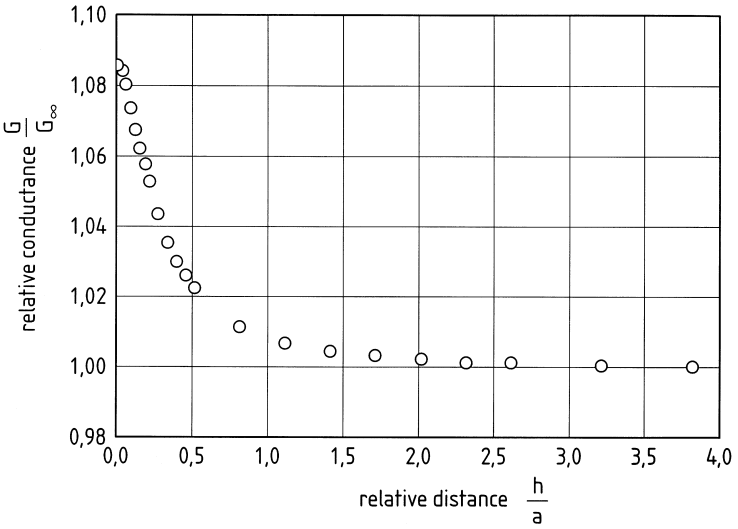

Figure 5. Dimensionless conductance between two wires as a function of the distance between the wire planes.

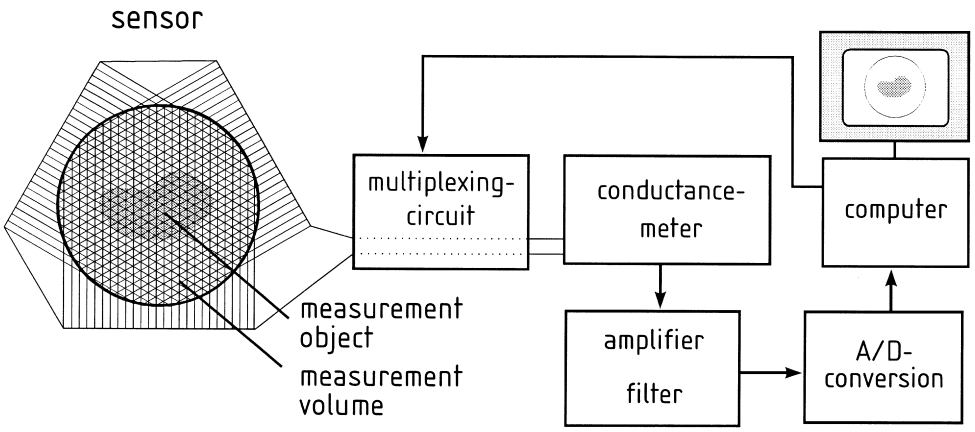

Figure 6. Schematic representation of the measuring chain for the new tomographic measurement technique.

figure 7. For a given initial distribution $\varepsilon(x, y)$ of the two phases [6] is used to calculate the measurement vector of all conductivities of all combinations of pairs of wires j:

$$G^{k*}_{\mathrm{R},j} = \frac{\sum_{(x,y)} (1(x, y)) S_j(x, y)}{\sum_{(x,y)} S_j(x, y)}. \qquad [6]$$

In [6] $S_j(x, y)$ is a weighting function or spatial amplification of the pair j at the point (x, y). The calculated vector of the projection is compared to the measured dimensionless conductivity:

$$\Delta G^{k*}_j = G^{*}_{\mathrm{M},j} G^{k*}_{\mathrm{R},j}. \qquad [7]$$

Using the difference ΔG^{k*}_j together with an algebraic optimizer (ART) a correction of the phase distribution is calculated. The optimization is done using

$$1(x, y)^k + ^1 = 1(x, y)^k + \frac{\Delta G^{k*}_j S_j(x, y)}{\sum_{(x,y)} S_j(x, y)}. \qquad [8]$$

For the algebraic reconstruction in Cartesian coordinates a number of projections are not located in parallel to the actual axises of the system. Therefore, errors for the discretization of the elements can be generated. This is schematically shown in figure 8(a). A correction of the property distribution in element (x_1, x_2) using the measurement value $\Phi_{\mathrm{M},1}$ can be compensated

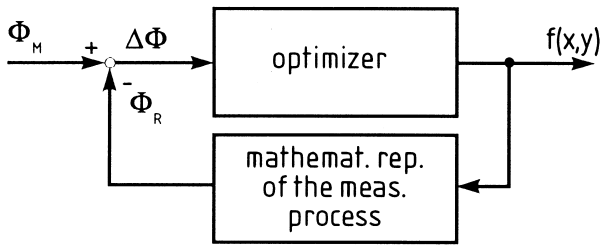

Figure 7. Schematic representation of the employed iterative reconstruction algorithm (ART).

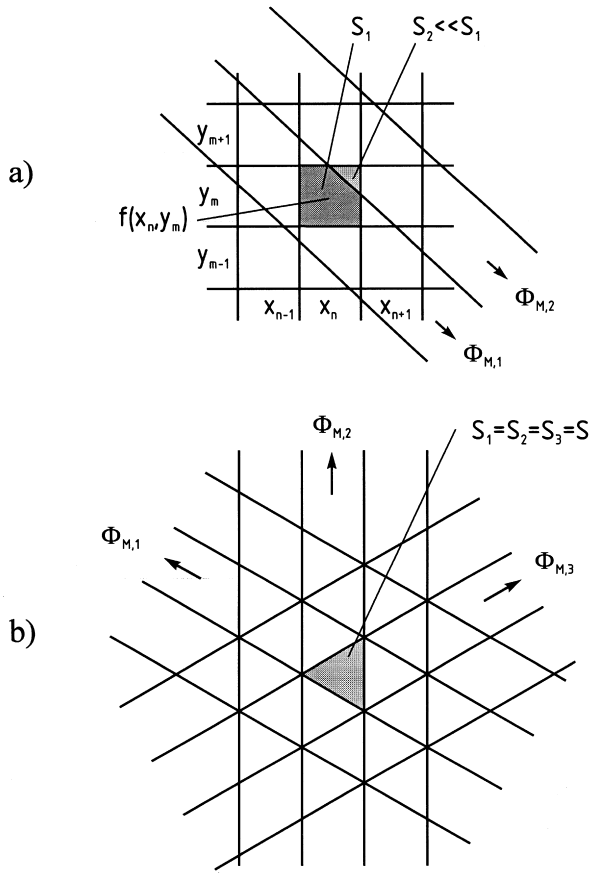

Figure 8. Representation of discretization in a cartesian (a) and a problem-oriented (b) coordinate system.

by a correction with the measurement $\Phi_{M,2}$. Additionally, the contribution of the element to the measurement $\Phi_{M,1}$ is small corresponding to the sensitivity $S_1(x, y)$. The amount of this contribution is in the same dimension as the measurement uncertainty of the whole integral measurement. For these reasons, in the present investigation the reconstruction is performed in a coordinate system which is fitted to the geometrical relations obtained by the wires in the measurement plane. This is shown schematically in figure 8(b). Due to the three different directions equilateral triangles are formed. The measurement plane is covered by a pattern of these equilateral triangles, each belonging to only one pair of wires per direction. Because all triangles have the same size their contributions to the measurements are all the same and the sensitivity of all elements is equal to unity.

To improve the reconstruction quality, the implementation of a priori knowledge into the reconstruction is necessary because of the underdetermination of the system of equations. The dimensionless values of the field distribution $\varepsilon(x, y)$ which are bigger than one or less than zero are set to one or zero automatically. The difference between the corrected and uncorrected values of the field function is redistributed to the other elements of the beam. If the dimensionless measurement value of a pair of wires is zero or one, all elements belonging to the beam must also have the same value. This information is not contained in [8]. Consequently, elements can be determined in the measurement plane for which the size of the field function is known for reconstruction. These elements are removed from the system of equations to be solved and its underdetermination is reduced. The conductances measured sequentially are shifted by the time correction proposed by Reinecke *et al.* (1994).

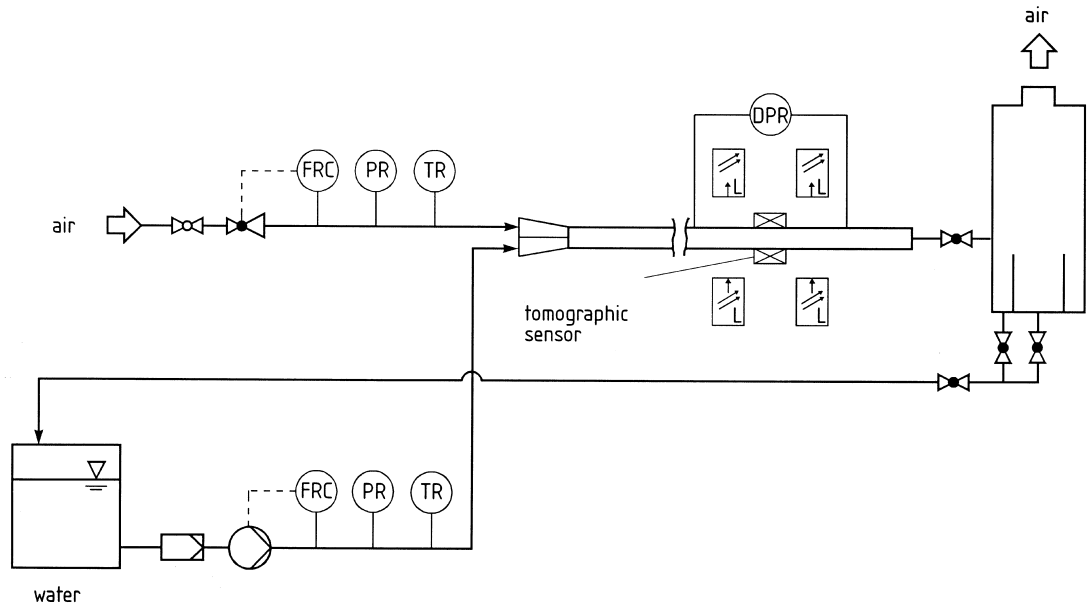

Figure 9. Representation of the experimental set-up.

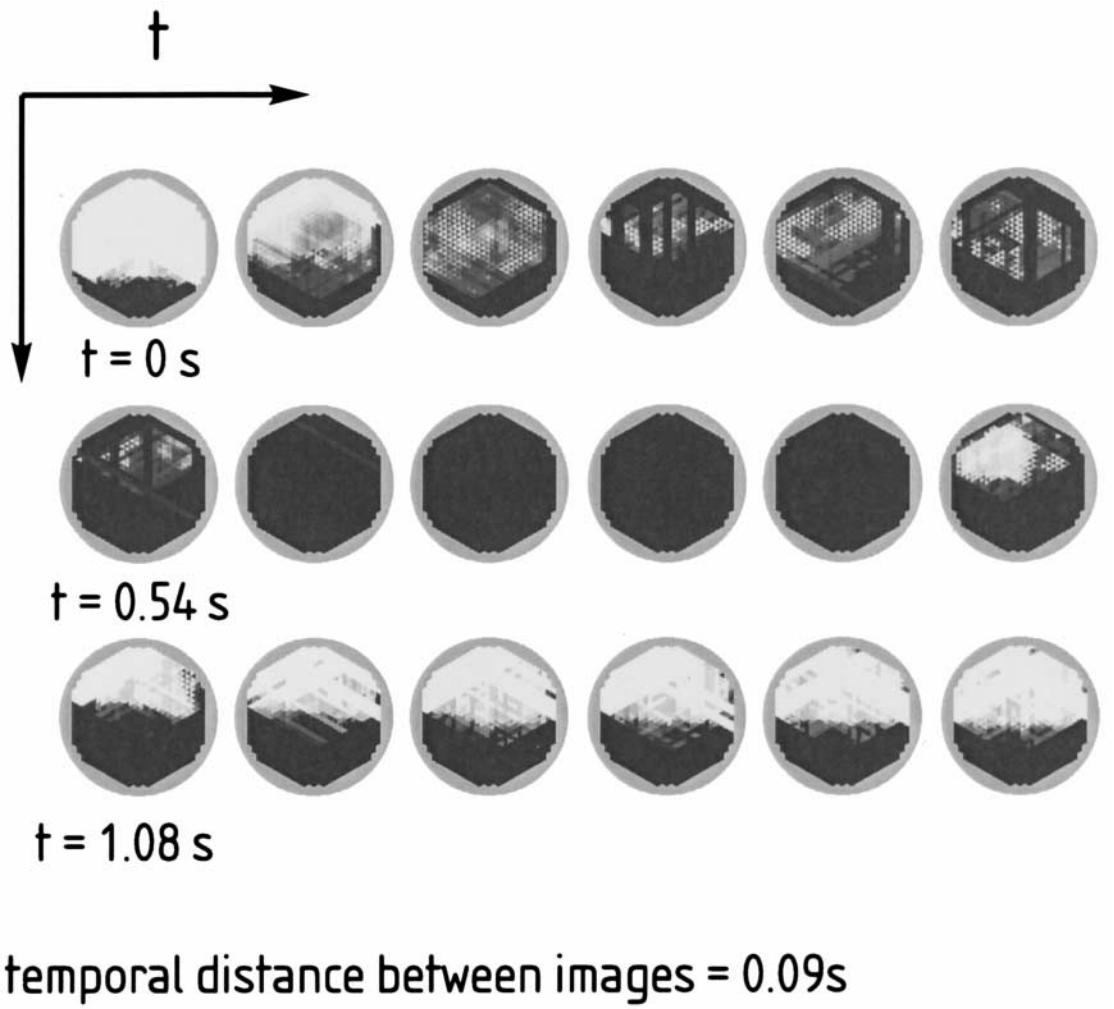

Figure 10. Phase distribution of a slug unit as a function of time.

4. DESCRIPTION OF THE EXPERIMENTAL SET-UP

The construction of the employed experimental set-up is represented schematically in figure 9. The test section consists of a horizontal, transparent pipe with the inner diameter of 59 mm. The length of the pipe is 48 m. The phases used are water and air. They are injected into the pipe by a nozzle as layers corresponding to their densities. At the outlet of the pipeline the phases are separated in the separator. The water is recirculated in a closed circuit. The volumetric flow rates of the phases are measured by orifices.

The tomographic sensor is installed into the pipeline at $l/d = 680$. For the tomographic imaging of the phase distribution, operating points of the two-phase flow are chosen for which the aerated slug flow is observed. The measurement is started shortly before the slug enters the measurement plane of the sensor. The measurement duration is 1.8 s with an image refresh rate of 110 pictures per second. For moderate slug velocities of 3.5 m/s and slug lengths of up to 1.5 m the phase distribution in the slugs is measured. No disturbance of the flow by the sensor is observed.

5. EXPERIMENTAL RESULTS

The measured and reconstructed phase distributions of a slug unit for different times are given in figure 10. Every tenth image is represented and the temporal distance between the represented phase distributions is therefore 0.09 s. The liquid phase is represented in dark shading, the gas phase in the bright one. The slug velocity is 3 m/s. Before the entry of the slug into the measurement plane, the gas phase occupies the biggest part of the measurement plane. While the slug front passes through the measurement cross-section the liquid hold-up increases rapidly. The gas phase is dispersed in the liquid phase in the center of the pipeline. The radial extension of the mixing zone reaches into the film zone before the slug. Behind the mixing zone, the slug body flows almost unaerated through the measurement plane. Individual gas bubbles reach the slug body from the mixing zone. They ascend to the top of the pipe due to their smaller density and the gas bubbles are transported to the slug end. At the slug end a liquid film remains at the pipe wall, which drains after the slug has passed. The liquid hold-up of the separated flow behind the slug is higher than before the slug. Additionally, the surface of the liquid film in the

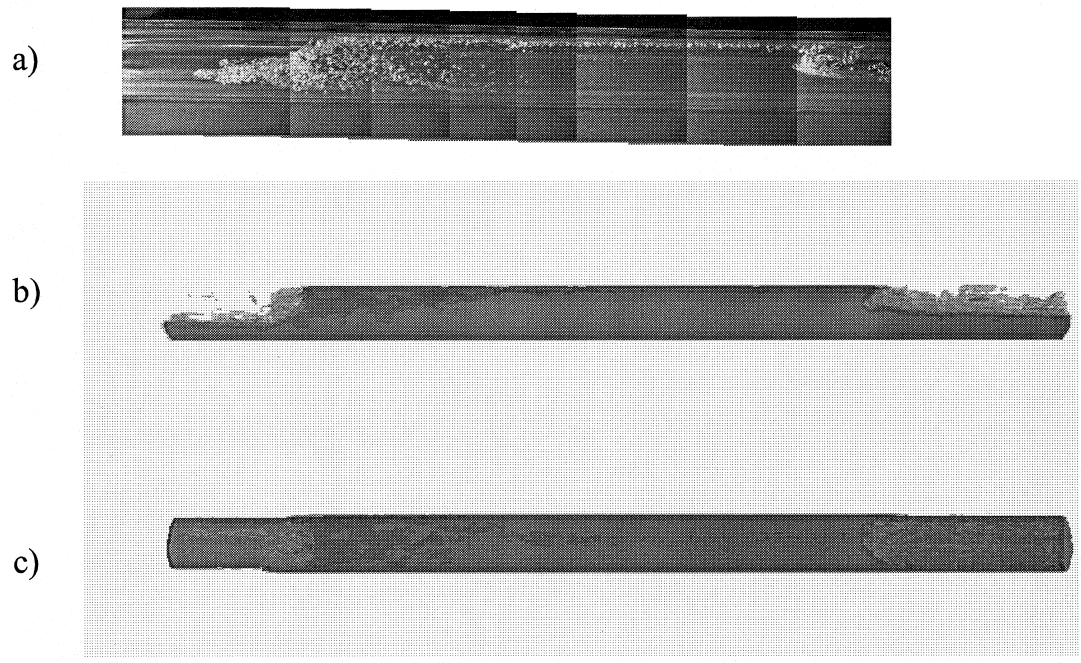

Figure 11. Photography of the slug (a) and Eulerian representation of the reconstructed slug unit (b), and (c).

stratified flow is wavier than in front of the slug. The liquid hold-up of the stratified flow after the slug decreases slowly to the amount in front of the slug front.

Three-dimensional data of the phase distribution in the slug unit is available with the aid of the tomographic measurements. By stacking the measured and reconstructed images, an Eulerian representation of the phase distribution of the slug is obtained. This Eulerian representation can be used to compare the measured and reconstructed slugs to visually observed ones. In figure 11(a) the side view of a slug is given. The direction of flow is from the right to the left. The mixing zone at the front of the slug is clearly visible. In order to compare this visual observation to the result of the tomographic measurement two Eulerian plots are given in figure 11(b) and (c). Two surfaces with different liquid contents are given in the figure. The surface colored darkly encloses the regions with a liquid hold-up over 0.5. The surface dyed brightly represents a liquid hold-up of 0.1. The slug is also represented in a side view, the direction of flow is from the right to the left. The surfaces are transparent so that the mixing zone in the slug front and

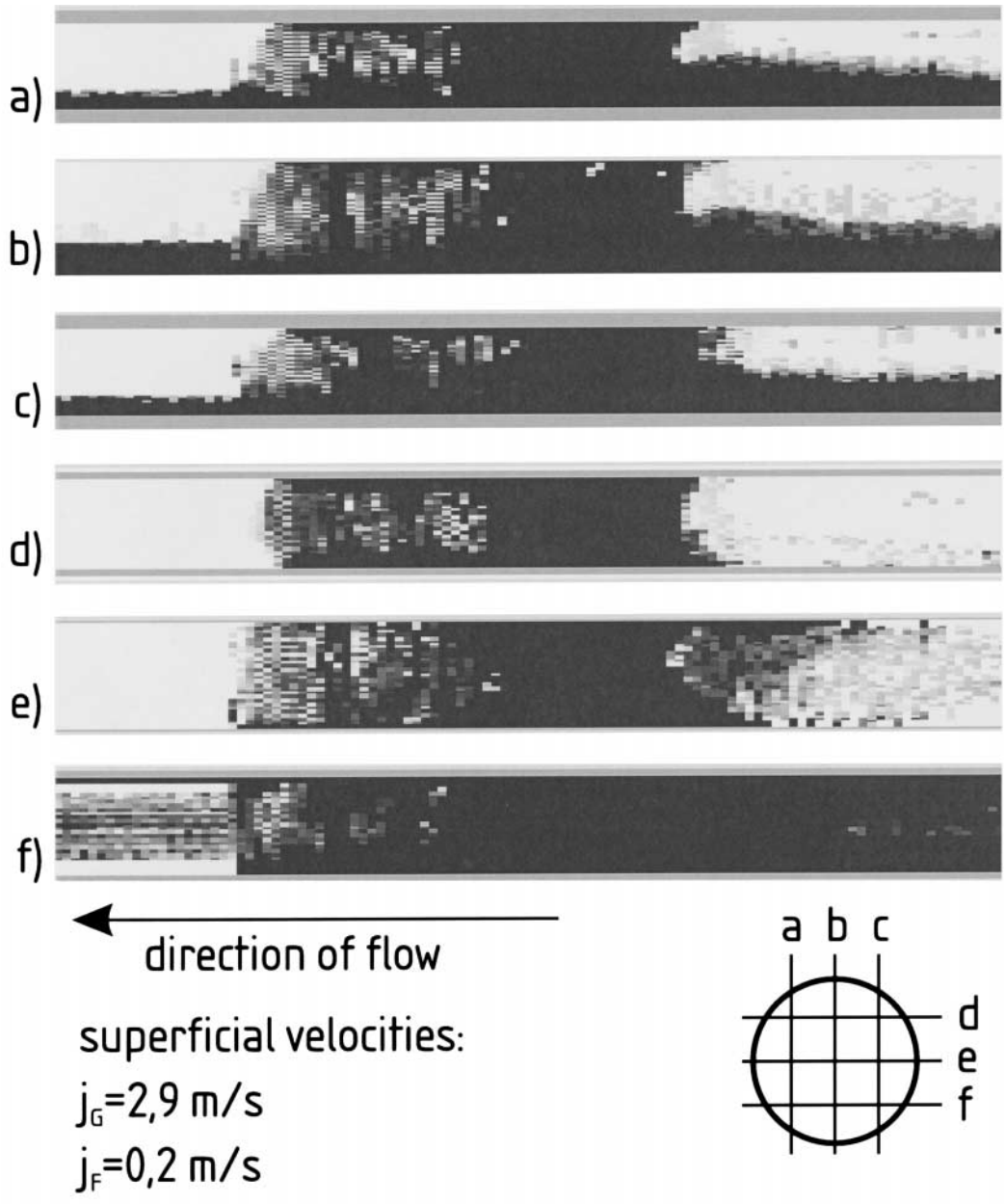

Figure 12. Images of the reconstructed slug unit.

the gas bubbles entrained from there can be observed. From visual comparison it is evident, that the characteristic slug properties, in particular the shape of the mixing zone, are captured using the tomographic technique.

Sectional views of the slug are represented in the figure 12(a)–(f). The corresponding position of the sectional views is to be taken from the rough draft in figure 12. The views in figure 12(a)–(c) are arranged vertically through the slug. The entrained gas bubbles and the liquid film remaining at the pipe wall behind the slug can be observed in this representation. Horizontal views of the slug are represented in figure 12(d)–(f). From this representation, the different heights of the liquid layer in the stratified flow in front of and behind the slug can be seen. The surface behind the slug is wavier than in front of the slug. The gas bubbles which are transported to the slug end oscillate in tangential direction.

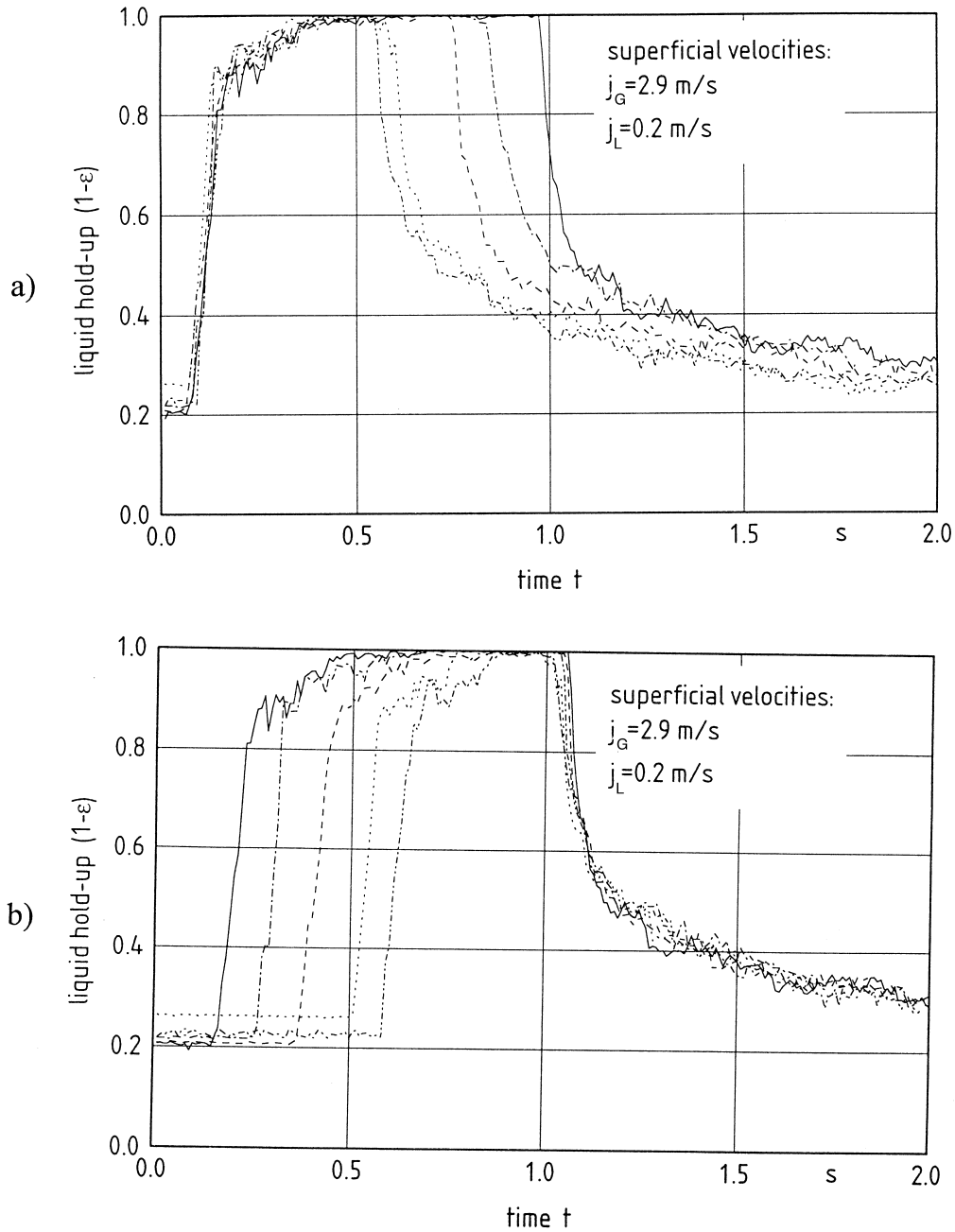

Figure 13. Liquid hold-up in the slug as a function of time.

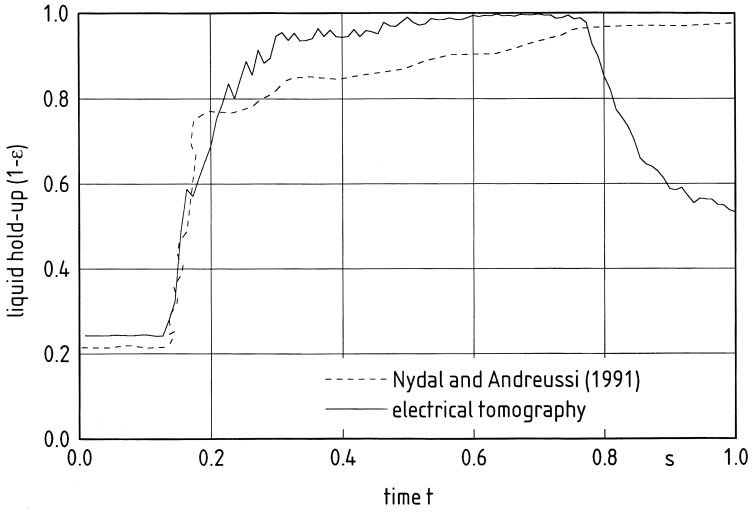

Figure 14. Comparison between the liquid hold-up measured by Nydal and Andreussi [14] and by electrical tomography.

From the reconstructed phase distribution, the liquid hold-up of the slug unit is calculated. The liquid hold-up of five different slugs is given in figure 13(a) as a function of time. The superficial gas velocity is 2.9 m/s and the superficial liquid velocity is 0.2 m/s. The liquid hold-up increased rapidly up to a value of 0.9 at the beginning of the slug front and then approaches slowly to the value of 1. The increase of the liquid hold-up in the slug front of all five slugs is identical. On the other hand, the length of the almost unaerated slug bodies of the five slugs is different. In figure 13(b) the time dependent liquid hold-ups of the five slugs are shifted so that the ends of the slugs coincide. The liquid hold-up of the five slugs as a function of time at the slug end is also identical. The representation of the liquid hold-up as a function of time given in figure 13 can be used to compare the results of the present investigation with results obtained by other authors. Time-plots in particular, are rarely given in publications. A very interesting experimental investigation is conducted by Nydal and Andreussi (1991). They use a conductance ring probe in a 49.7 mm i.d. pipe to measure the time-varying liquid hold-up in the slug flow. The measurements are conducted for artificial single slugs generated in the slight inclined horizontal pipe. Therefore, the experimental conditions are similar but not identical to the present ones. In figure 14 the results for the liquid hold-up as a function of time for two measurements conducted in the present study and by Nydal and Andreussi (1991) are compared. The conditions are similar with a slug velocity in the investigations by Nydal and Andreussi (1991)

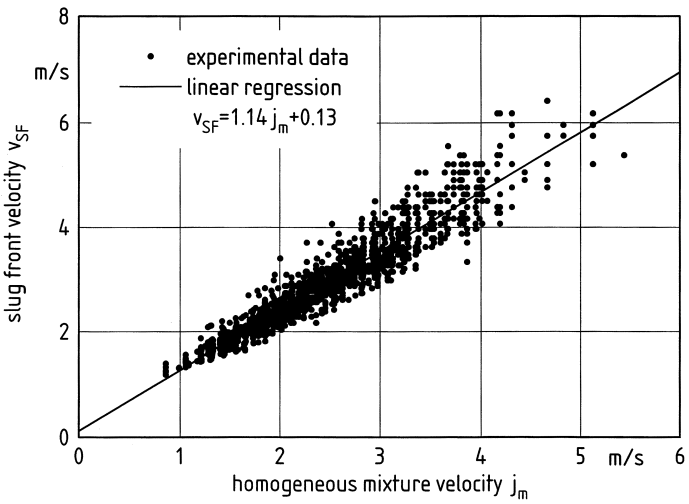

Figure 15. Slug velocity as a function of the mixture velocity.

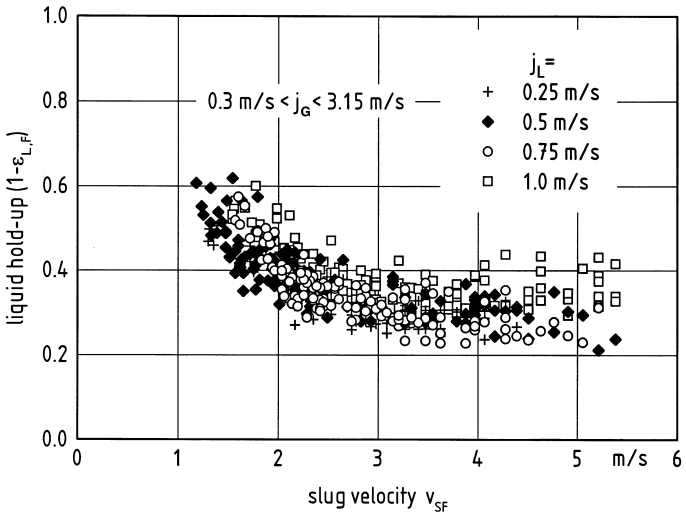

Figure 16. Liquid hold-up in the film zone as a function of the slug velocity.

being 2.7 m/s and 3.8 m/s in the present investigation. The agreement is reasonable given the statistical nature of the flow and the significantly different experimental conditions in the two studies.

In further investigations the liquid hold-up in different sections of the slug unit is measured as a function of the slug velocity. To measure the velocity of the slug front a light barrier technique is used. In figure 15 the slug velocity is plotted as a function the mixture velocity. A linear correlation for the data can be found as

$$v_{SF} = C_0 j_m + v_0 = 1.14 j_m + 0.13. \quad [9]$$

The results for the two parameters are comparable to correlations found by other authors, for example Gregory and Scott (1969) ($C_0 = 1.35$), Dukler and Hubbard (1975) ($C_0 = 1.24$–1.3), Nicholson *et al.* (1978) ($C_0 = 1.128$–1.196, $v_0 = 0.27$–0.28 m/s) and Jepson (1987) ($C_0 = 1.4$–1.5).

The liquid hold-up in the different sections of the slug is calculated from the reconstructed phase distributions in the cross-sectional area of the pipe. In figure 16 the liquid hold-up in the film zone directly in front of the individual slugs is plotted as a function of the velocity of the slug front. The superficial gas velocity and the superficial liquid velocity are varied from

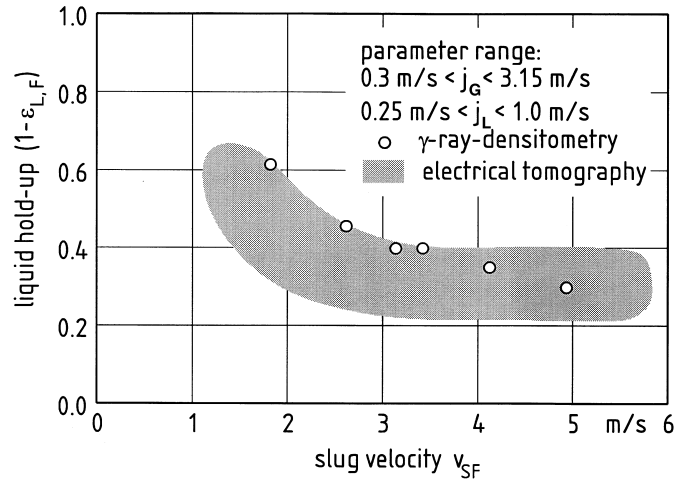

Figure 17. Comparison of results for the liquid hold-up in the film zone by electrical tomography and γ-ray-densitometry.

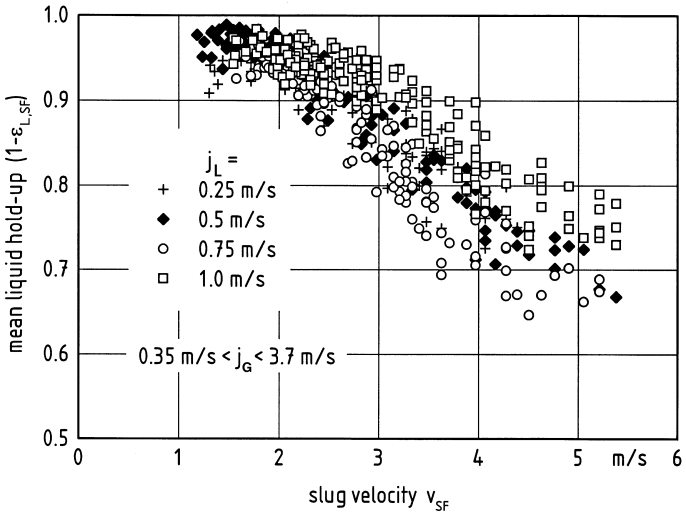

Figure 18. Liquid hold-up in the mixing zone as a function of the slug velocity.

$j_G = 0.35$ to 3.7 m/s and from $j_G = 0.25$ to 1.0 m/s, respectively. Due to the statistical nature of two phase flows there is a scatter in the experimental data. For small velocities of the slug front the liquid hold-up is decreasing with increasing slug velocity. For slug velocities greater than 2 m/s the liquid hold-up in the film zone is nearly independent of the slug velocity. There is no dependency on the superficial velocity of the liquid. It makes no difference if the increase in slug velocity is caused by an increase of the liquid or the gas flow rate. The film thickness is only a function of the slug velocity or is constant for slug velocities over 2 m/s, respectively. A comparison of the liquid hold-up in the film zone measured by electrical tomography and by γ-ray-densitometry is given in figure 17. The γ-ray-densitometry results are obtained in the same experimental facility. The range of the liquid hold-up measured by the tomographic measurement technique is shaded in light gray. The single data points plotted in the diagram are average values of several slugs and are calculated from measurements of the liquid hold-up in the whole film zone by γ-ray-densitometry. Due to this, there is a systematic deviation between the γ-ray-densitometry results and the tomography results. Because the liquid hold-up in the film zone in front of the slug is smaller than behind a slug the average values of the liquid hold-up obtained by γ-ray-densitometry tend to be greater.

In figure 18 the mean liquid hold-up in the slug front is shown as a function of the slug velocity. To calculate the mean liquid hold-up in the slug front only the first section of the whole

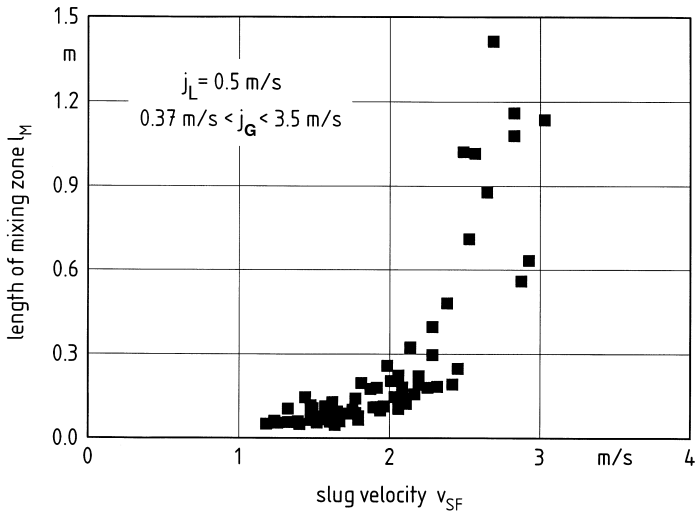

Figure 19. Length of the mixing zone as a function of the slug velocity.

slug is considered. The length of this section is set to 0.6 m. Due to this definition of the mean liquid hold-up in the slug front a representative value of the aeration of the slug is obtained. For small slug front velocities below $v_{SF} = 2$ m/s there is no aeration of the slug. Over 2 m/s the liquid hold-up decreases with increasing slug velocity. First gas bubbles are entrained into the slug front. With a further increase the liquid hold-up is decreasing. This is due to the higher void fraction in the slug front and due to the elongation of the aerated front section of the slug. A dependency on the injected liquid flow rate is not determined. The length of the aerated front section of the slug is shown in figure 19. The superficial velocity of the liquid is $j_L = 0.5$ m/s. A significant entrainment of gas into the slug front starts at $v_{SF} = 2$ m/s. For $v_{SF} = 3$ m/s the whole slug is aerated.

From the experimental data it is obvious that there is no influence of the composition of the injected fluids on the slug properties. The main parameter is the velocity of the slugs which is directly related to the sum of the superficial velocities of the injected fluids. The most interesting range of slug velocities is between 2 and 3 m/s. In this interval the aeration of the liquid slugs takes place. For velocities greater than 3 m/s the decrease of the film thickness between the slugs has ceased, too.

6. CONCLUSION

Slug flow is the predominant flow regime for two-phase flow of gases and liquids through horizontal pipelines. It is characterized by alternating gas bubbles and liquid slugs flowing through the pipeline. Gas is dispersed into the slug moving over a liquid film due to the high flow velocities. To calculate the slug velocity and the pressure loss of the flow the knowledge of the spatial distribution of the gas phase in the slug body is necessary.

In an experimental investigation, an electrical tomographic measurement technique is used to measure the spatial phase distribution of the gas phase in the slug. Features of the technique are high local and temporal resolution. The sensor employed consists of parallel wires arranged in three different parallel planes. The conductance is measured between the pairs of parallel wires. The conductance is directly proportional to the liquid hold-up between the wires. From the measured values, the phase distribution is calculated by means of an iterative reconstruction algorithm. The reconstruction quality is corrected by introduction of a priori knowledge. The temporal resolution is 0.009 s and the spatial resolution is less than 0.1% of the cross-sectional area.

The measurements are performed in a horizontal two-phase flow with slug velocities of up to 3 m/s. For these superficial velocities liquid slugs of different length are formed. The dispersion of the gas phase is limited to the slug front. Within the slug body, gas bubbles are transported to the top of the pipe coalescing with the bubble following the slug.

Acknowledgements—The authors wish to thank the DFG for the financial aid awarded within the framework "transients in multiphase systems with one or several components".

REFERENCES

Abdullah, M. Z. (1993) Electrical impedance tomography for imaging conducting mixtures in hydrocyclone separators. Ph.D. Thesis. University of Manchester, Manchester, UK.

Adams, M. F. and Anderson, A. P. (1982) Synthetic aperture tomographic imaging for microwave diagnostics. *Proc. Inst. Elec. Eng.* **129,** 83–88.

Andreussi, P. and Bendiksen, K. (1989) An investigation of void fraction in liquid slugs for horizontal and inclined gas–liquid pipe flow. *Int. J. Multiphase Flow* **15,** 937–946.

Azzopardi, B. J., Govan, A. H. and Hewitt, G. F. (1985) Two-phase slug flow in horizontal pipes.. *Preprints Vol. 2, Symposium Pipelines.* Institution of Chemical Engineers European Branch, Utrecht, pp. 213–225.

Barnea, D. and Brauner, N. (1985) Holdup for the liquid slug in two-phase intermittent flow. *Int. J. Multiphase Flow* **11,** 43–49.

Beggs, H. D. and Brill, J. P. (1973) A study of two-phase flow in inclined pipes. *Trans. AIME 255, J. Petroleum Tech.* **25,** 607–617.

Delhaye, J. M. (1978) Optical methods in two-phase flow. *Proc. of the Dynamic Flow Conference Marseille.*

Dukler, A. E. and Hubbard, M. G. (1975) A model for gas–liquid slug flow in horizontal and near horizontal tubes. *Ind. Eng. Chem. Fund.* **14,** 337–347.

Gladden, L. F. (1994) NMR in chemical engineering. *Chem. Eng. Sci.* **49,** 3339–3408.

Gregory, G. and Scott, D. S. (1969) Correlation of the liquid slug velocity and frequency in horizontal cocurrent gas liquid flow. *AIChE J.* **15,** 933–935.

Gregory, G. A., Nicholson, M. K. and Aziz, K. (1978) Correlation of the liquid volume fraction in the slug for horizontal gas–liquid slug-flow. *Int. J. Multiphase Flow* **4,** 33–39.

Herm-Stapelberg, H. and Mewes, D. (1994) The pressure loss and slug frequency of liquid–liquid–gas slug flow in horizontal pipes. *Int. J. Multiphase Flow* **20,** 285–303.

Hewitt, G. F. (1991) Phenomena in horizontal two-phase flow. *Proc. Int. Conf. on Multiphase Flows, Tsukuba, Japan.*

Ikeda, T., Kotani, K., Maeda, Y. and Kohno, H. (1983) Preliminary study on application of X-ray CT scanner to measurement of void fraction in steady state two-phase flows. *J. of Nuclear Science and Technology* **20,** 1–12.

Jepson, W. P. and Taylor, R. E. (1993) Slug flow and its transitions in large-diameter horizontal pipes. *Int. J. Multiphase Flow* **19,** 411–420.

Jepson, W. (1987) The flow characteristics in horizontal slug flow. Paper F2. *3rd Int. Conf. on Multiphase Flow, The Hague.*

Jones, O. C. and Delhaye, J. M. (1976) Transient and statistical measurement techniques for two-phase flows: a critical review. *Int. J. Multiphase Flow* **3,** 89–116.

Mewes, D. and Fellhölter, A. (1993) Observation of mixing phenomena in wind tunnels by optical tomography. In *Proc. ECAPT '93, Karlsruhe, Germany, Process Tomography—A Strategy for Industrial Exploitation*, eds M. S. Beck, E. Campogrande, M. Morris, R. C. Waterfall and R. A. Williams, pp. 289–292.

Mewes, D., Ostendorf, W., Haarde, W. and Friederich, M. (1989) Tomographic measurement techniques for process engineering studies. In *Handbook of Heat and Mass Transfer*, ed. N. P. Cheremisinoff, Vol. 3, pp. 951–1021. Gulf Publishers.

Nädler, M. and Mewes, D. (1995a) The effect of gas injection on the flow of immiscible liquids in horizontal pipes. *Chem. Eng. Technology* **18,** 156–165.

Nädler, M. and Mewes, D. (1995b) Effects of liquid viscocity on the phase distribution in horizontal gas–liquid slug flow. *Int. J. Multiphase Flow* **21,** 253–266.

Nicholson, M., Aziz, K. and Gregory, G. A. (1978) Intermittent two-phase flow in horizontal pipes: predictive models. *Can. J. Chem. Engng* **56,** 653–663.

Nydal, O. J. and Andreussi, P. (1991) Gas entrainment in a long liquid slug advancing in a near horizontal pipe. *Int. J. Multiphase Flow* **17,** 179–189.

Ostendorf, W. and Mewes, D. (1988) Measurement of three-dimensional unsteady temperature profiles in mixing vessels by optical tomography. *Chem. Eng. Technology* **11,** 148–155.

Ozawa, M., Akagawa, K. and Skagucchi, T. (1989) Flow instabilities in parallel-channel flow systems of gas–liquid two-phase mixtures. *Int. J. Multiphase Flow* **15,** 639–657.

Reinecke, N. and Mewes, D. (1994) Resolution enhancement for multi-electrode capacitance sensors. In *Proc. ECAPT '94, Oporto, Portugal, Process Tomography—A Strategy for Industrial Exploitation*, eds M. S. Beck, E. Campogrande, E. A. Hammer, M. Morris, R. C. Waterfall and R. A. Williams, pp. 50–61.

Reinecke, N., Boddem, M. and Mewes, D. (1994) Improvement of tomographic reconstructions by time-correction of sequential measurements. In *Proc. ECAPT '94, Oporto, Portugal, Process Tomography—A Strategy for Industrial Exploitation*, eds M. S. Beck, E. Campogrande, E. A. Hammer, M. Morris, R. C. Waterfall and R. A. Williams, pp. 381–392.

Rowland, S. W. (1979) Computer implementation of image reconstruction formulas. In *Image Reconstruction from Projections Implementation and Applications*, ed. G. T. Herman, pp. 9–80. Springer, Berlin.

Simons, J. R. S., Seville, J. P. K., Broadbent, C. J., Bridgwater, J., Parker, D. J., Beynon, T. D. and Hawkesworth, M. R. (1993) The study of particle motion in fluidised beds using positron emission tomography. In *Proc. ECAPT '93, Karlsruhe, Germany, Process Tomography—A Strategy for Industrial Exploitation*, eds M. S. Beck, E. Campogrande, M. Morris, R. C. Waterfall and R. A. Williams, pp. 261–264.

Spedding, P. L., O'Hare, K. D. and Spence, D. R. (1988) Prediction of holdup in two-phase flow. *Particulate Phenomena and Multiphase Transport*. Hrsg. T. N. Veziroglu, Hemisphere Publishing Corp., London.

Wang, M., Dickin, F. J., Williams, R. A., Waterfall, R. C. and Beck, M. S. 1994. Electrical resistance tomography on metal walled vessels. *Proc. ECAPT '94*, Oporto, Portugal, *Process Tomography—A Strategy for Industrial Exploitation*. eds M. S. Beck, E. Campogrande, E. A. Hammer, M. Morris, R. C. Waterfall and R. A. Williams, pp. 183–170.

Xie, C. G., Reinecke, N., Beck, M. S., Mewes, D. and Williams, R. A. (1995) Electrical tomography techniques for process engineering applications. *Chem. Eng. J.* **56,** 127–133.